


LETTER

Open Access



# Seismicity controlled by resistivity structure: the 2016 Kumamoto earthquakes, Kyushu Island, Japan

Koki Aizawa<sup>1\*</sup> , Hisafumi Asaue<sup>2</sup>, Katsuaki Koike<sup>3</sup>, Shinichi Takakura<sup>4</sup>, Mitsuru Utsugi<sup>5</sup>, Hiroyuki Inoue<sup>5</sup>, Ryokei Yoshimura<sup>6</sup>, Ken'ichi Yamazaki<sup>7</sup>, Shintaro Komatsu<sup>7</sup>, Makoto Uyeshima<sup>8</sup>, Takao Koyama<sup>8</sup>, Wataru Kanda<sup>9</sup>, Taro Shiotani<sup>5</sup>, Nobuo Matsushima<sup>4</sup>, Maki Hata<sup>4</sup>, Tohru Yoshinaga<sup>10</sup>, Kazunari Uchida<sup>1</sup>, Yuko Tsukashima<sup>1</sup>, Azusa Shito<sup>1</sup>, Shiori Fujita<sup>1</sup>, Asuma Wakabayashi<sup>1</sup>, Kaori Tsukamoto<sup>1</sup>, Takeshi Matsushima<sup>1</sup>, Masahiro Miyazaki<sup>1,6</sup>, Kentaro Kondo<sup>1</sup>, Kanade Takashima<sup>1</sup>, Takeshi Hashimoto<sup>1,11</sup>, Makoto Tamura<sup>1,2</sup>, Satoshi Matsumoto<sup>1</sup>, Yusuke Yamashita<sup>1,7</sup>, Manami Nakamoto<sup>1</sup> and Hiroshi Shimizu<sup>1</sup>

## Abstract

The  $M_{\text{JMA}}$  7.3 Kumamoto earthquake that occurred at 1:25 JST on April 16, 2016, not only triggered aftershocks in the vicinity of the epicenter, but also triggered earthquakes that were 50–100 km away from the epicenter of the main shock. The active seismicity can be divided into three regions: (1) the vicinity of the main faults, (2) the northern region of Aso volcano (50 km northeast of the mainshock epicenter), and (3) the regions around three volcanoes, Yufu, Tsurumi, and Garan (100 km northeast of the mainshock epicenter). Notably, the zones between these regions are distinctively seismically inactive. The electric resistivity structure estimated from one-dimensional analysis of the 247 broadband (0.005–3000 s) magnetotelluric and telluric observation sites clearly shows that the earthquakes occurred in resistive regions adjacent to conductive zones or resistive-conductive transition zones. In contrast, seismicity is quite low in electrically conductive zones, which are interpreted as regions of connected fluids. We suggest that the series of the earthquakes was induced by a local accumulated stress and/or fluid supply from conductive zones. Because the relationship between the earthquakes and the resistivity structure is consistent with previous studies, seismic hazard assessment generally can be improved by taking into account the resistivity structure. Following on from the 2016 Kumamoto earthquake series, we suggest that there are two zones that have a relatively high potential of earthquake generation along the western extension of the MTL.

**Keywords:** Magnetotellurics, Resistivity structure, 2016 Kumamoto earthquake, Futagawa fault, Hinagu fault, Structural control, Aso volcano, Kuju volcano, Tsurumi volcano, Median Tectonic Line

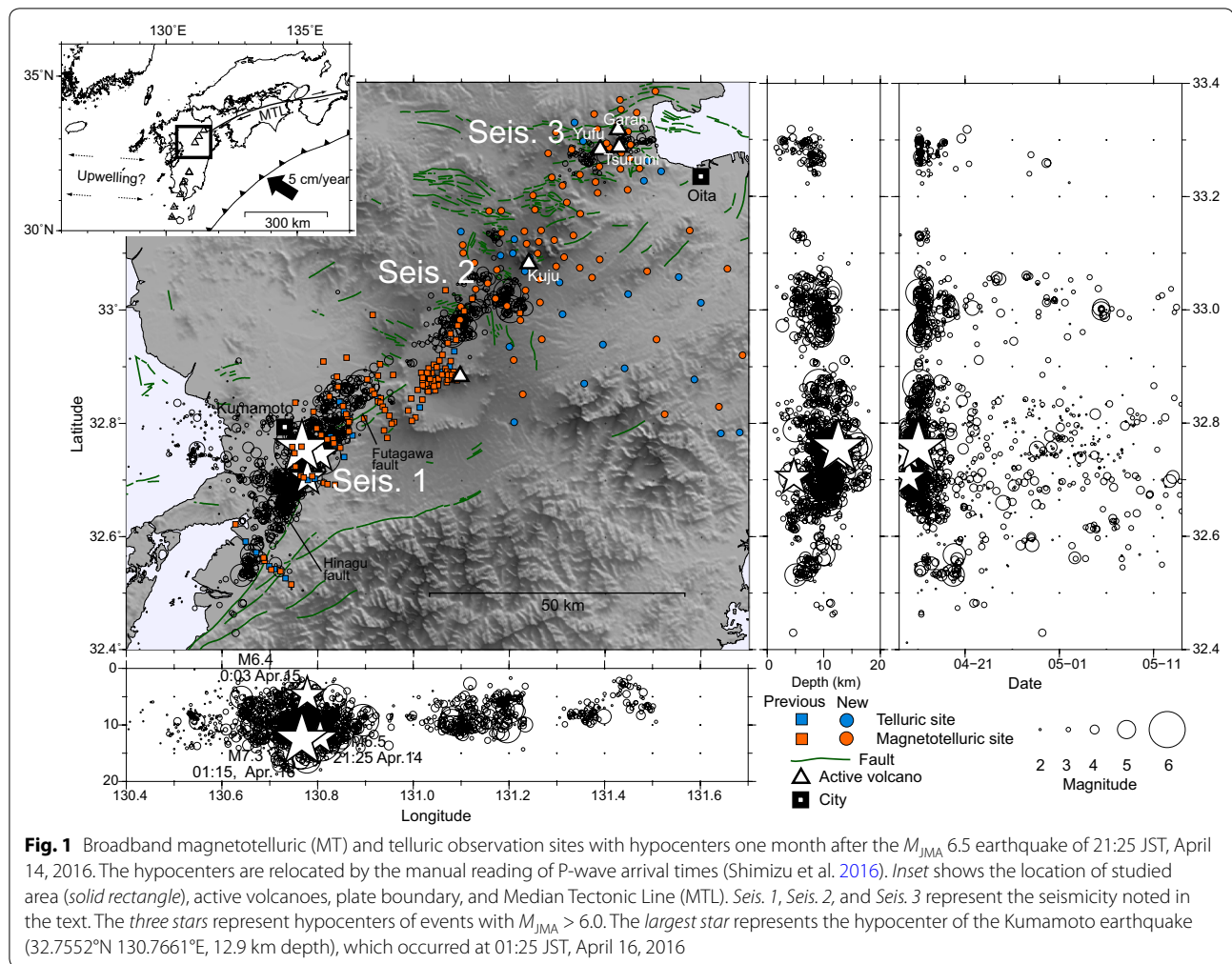
## Introduction

The  $M_{\text{JMA}}$  7.3 (Mw 7.0) Kumamoto earthquake occurred at 1:25 JST (Japan Standard Time) on April 16, 2016, which followed the nearby  $M_{\text{JMA}}$  6.5 (Mw 6.2) earthquake at 21:26 JST on April 14, 2016. The dextral strike-slip earthquake rupture propagated mainly in an ENE direction from the hypocenter to the west of Aso volcano

along the Futagawa fault (e.g., Asano and Iwata 2016; Kobayashi et al. 2016) (Fig. 1). One prominent feature of this earthquake sequence is the spatial distribution of the events: These are not limited to aftershocks in areas around the rupture zone, but include triggered seismic events located 50–100 km from the mainshock (Shimizu et al. 2016). The active seismicity can be divided into three regions: Seis. 1, around the main faults; Seis. 2, the northern part of Aso volcano; and Seis. 3, the region around the three volcanoes, Yufu, Tsurumi, and Garan (Fig. 1). Since the earthquakes around Seis. 2 and Seis. 3 began

\*Correspondence: aizawa@sevo.kyushu-u.ac.jp

<sup>1</sup> Institute of Seismology and Volcanology, Faculty of Science, Kyushu University, 2-5643-29 Shin'yama, Shimabara, Nagasaki 855-0843, Japan  
Full list of author information is available at the end of the article



immediately after the Kumamoto earthquake, earthquakes in these regions are considered to be triggered by the mainshock of *Seis. 1*. Subsequent earthquakes not only were small earthquakes, but also included moderate earthquakes ( $>M_{JMA}$  3.5) that totaled 230 events by May 8, 2016. The concern for future earthquakes has been derived from the fact that the NE–SW-trending line along which the earthquakes occur corresponds to the possible western extension of the Median Tectonic Line (MTL), which is the longest and most active arc-parallel, right-lateral, strike-slip fault system in the Japan arc (Fig. 1). The oblique subduction of Philippine Sea Plate (Seno et al. 1993) induces a shear stress in the vicinity of the MTL and separates the fore-arc sliver from the crust of the arc at depth (Kamata and Kodama 1994; Miyazaki and Heki 2001; Tabei et al. 2002). Along the western extension of the MTL in Kyushu, the shear stress is found to be partly released by deformation (Nishimura and Hashimoto 2006; Wallace et al. 2009; Matsumoto

et al. 2015). In 1975,  $M_{JMA}$  6.1 and  $M_{JMA}$  6.4 earthquakes occurred within 3 months in the region of *Seis. 2*, and between *Seis. 2* and *Seis. 3*, respectively (Yamashina and Murai 1975). Along the MTL, three M7 class earthquakes occurred within 4 days in 1596 (Kanaori et al. 1994; Toda et al. 2015). Therefore, it is reasonable to be concerned about the occurrence of large earthquakes around the MTL and its western extension.

In addition to the shear stress along the western extension of the MTL, the island of Kyushu is considered to be influenced by tectonics stress associated with back-arc spreading (e.g., Seno 1999) (Fig. 1). Geomagnetic depth sounding research supports a region of increased electrical conductivity in the mantle below the back-arc side of Kyushu (Handa et al. 1992; Shimoizumi et al. 1997). Furthermore, the series of Kumamoto earthquakes, including those that were triggered by the initial series, occurred in a graben structure (Matsumoto 1979; Kamata 1989; Handa 2005) and around the active

volcanoes. Such complex tectonic settings suggest complex subsurface structures that may be related to the characteristic seismicity. Because electrical resistivity is sensitive to the presence of fluids, and subsequently the elasticity of the media, it is important to investigate how resistivity structures relate to earthquake generation (Ogawa et al. 2001; Fujinawa et al. 2002; Goto et al. 2005; Guerer and Bayrak 2007; Wannamaker et al. 2009; Yoshimura et al. 2009; Ichihara et al. 2011, 2014, 2016; Ogawa et al. 2014; Kaya et al. 2013). To investigate the relationship between earthquakes and electrical resistivity structure, we gathered and analyzed the broadband (typically 0.003–10,000 s) magnetotelluric (MT) and telluric data, which resolve the resistivity structure from the surface to the depth of the upper mantle.

### Broadband magnetotelluric data

We conducted the MT and telluric data surveys during 2014–2015 in the vicinity of Aso caldera, in the region of triggered seismicity (Seis. 2 and Seis. 3), and to the south of the city of Oita. In addition, we used previously published MT and telluric data from the region of the main shock of the 2016 Kumamoto earthquake (Asaue et al. 2004, 2007, 2012) and around Aso volcano (Takakura et al. 2000; Asaue et al. 2006; Hata et al. 2016). The number of sites used in this study amounted to 247, including 94 unpublished new data.

For the 2015 MT survey around Aso volcano, the MT data were measured by the Phoenix MTU5 systems (telluric and geomagnetic field observations). The MT response functions were calculated using the SSMT2000 program (Phoenix Geophysics Ltd). Typically, recording duration was 2–3 nights. We also employed remote-reference processing (Gamble et al. 1979) using MT data recorded at the Esashi Magnetic Observatory, which is located about 1000 km northeast of Aso volcano.

For the 2014–2015 MT surveys around Seis. 2 and Seis. 3, and south of Oita, the MT data were measured with a Metronix ADU07e system (telluric and geomagnetic field observations) and the NT System Design ELOG1K (telluric only observations). Typically, recording duration was 10 days. MT response functions were calculated using a robust estimation code (Chave and Thomson 2004). At the telluric observation sites, geomagnetic data from the nearest sites were used for calculations. In all calculations, notch filtering was applied to the time series data to reduce anthropogenic 60 Hz noise and its odd-order overtones (Aizawa et al. 2013). We employed remote-reference processing (Gamble et al. 1979) for periods <10 s, using MT data recorded at other MT sites. For the periods >10 s, the 1-Hz-sampled geomagnetic data recorded at the Kakioka Magnetic Observatory (located about 1000 km east-northeast of Kyushu) were used for

remote-reference processing. Using these approaches, we obtained MT response functions across a broad (0.005–3000 s) range of periods. The periods of the MT response functions vary slightly among datasets due to differences in sampling frequencies. We interpolated the MT response functions and errors in the frequency domain using a cubic spline function. The MT response functions were then defined for specific frequencies.

### Resistivity structure determined by one-dimensional analysis

Recent development of 3-D MT inversion codes by finite difference methods (e.g., Siripunvaraporn and Egbert 2009; Kelbert et al. 2014) allows us to deduce three-dimensional (3-D) resistivity structure. In our dataset, the sites are mainly located along five lines across the Futagawa and Hinagu faults, with the overall region located along an elongated NE–SW region (Fig. 1). Applying 3-D inversion codes to such uneven site locations requires the construction of a huge horizontal mesh and subsequently has extensive memory and computational time requirements, even with a high-end workstation. In this study, as an alternative, we have adapted a one-dimensional (1-D) inversion routine for the data at each site. The apparent resistivity and the phase of the sum of the squared elements (ssq) invariant impedance (Szarka and Menvielle 1997; Rung-Arunwan et al. 2016) are inverted with Occam's algorithm (Constable et al. 1987). The ssq impedance ( $Z_{ssq}$ ) is defined as,

$$Z_{ssq} = \sqrt{\frac{Z_{xx}^2 + Z_{xy}^2 + Z_{yx}^2 + Z_{yy}^2}{2}},$$

where  $Z_{xx}$ ,  $Z_{xy}$ ,  $Z_{yx}$ , and  $Z_{yy}$  are the components of the impedance tensor. Commonly used determinant impedances are generally biased downward by the presence of galvanic distortion, while ssq impedances are robust with respect to distortion and are therefore suitable for obtaining a first-order approximation of the regional structure (Rung-Arunwan et al. 2016).

In the 1-D inversion, we assigned error of  $\pm 10\%$  to each ssq impedance (equivalent to  $\pm 0.0434$  in log apparent resistivity and  $\pm 2.85^\circ$  in phase), with the exception of the dead-band data from 6.4 to 25.6 s, which were assigned larger error of  $\pm 30\%$ . In addition, outliers from smooth sounding curves were judged visually and were assigned errors larger than  $\pm 30\%$ . Using these procedures, we estimated the smoothest resistivity structure in which the model response fit the data to an RMS tolerance of 1.0. Figures 2 and 3 show the comparison of the apparent resistivity and phase maps of the observed data (obs) with the calculated response (clc). Overall, the observed data are well explained by the estimated resistivity structure.

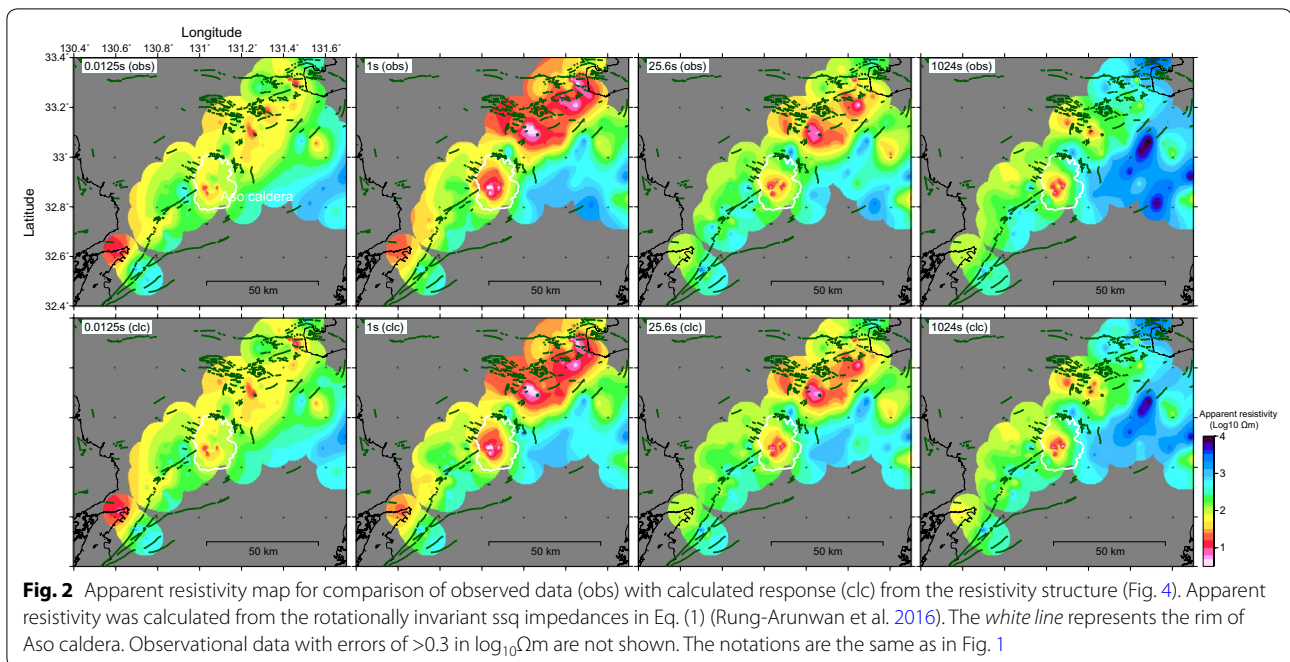


Figure 4 shows the estimated resistivity structure. Strictly speaking, it is difficult to evaluate how well 1-D analysis using ssq impedance approximates regional structure. In this study, we calculated the skew angle ( $\beta$ ) of the magnetotelluric phase tensor (Caldwell et al. 2004) (Fig. 5) to check for the presence of strong 3-D features produced by the true resistivity structure: Large  $|\beta|$  indicates the presence of a 3-D resistivity structure around a site. Although large  $|\beta|$  values are present locally, large parts of the studied area show  $|\beta| < 10^\circ$  to periods of 25.6 s, which correspond to a 12.5 km skin depth in a 30- $\Omega\text{m}$  half-space. At longer periods, to 1024 s, areas of  $|\beta| > 10^\circ$  are present, especially at the north flank of Kuju volcano. It should be noted here that the zones of large  $|\beta|$  approximately correspond to zones where the estimated resistivity significantly changes horizontally. This implies that the 1-D analysis might approximate the 3-D structure, even in a zone of large  $|\beta|$ . Full 3-D analysis will be the subject of future work.

In a broad sense, obtained resistivity structure (Fig. 4) shows a structural boundary across the Hinagu and Futagawa faults at depths of 1 and 4 km (i.e., the northwestern parts of the faults are conductive, while the southeastern parts are resistive), as stated in Asaue et al. (2012). A similar feature is also found between Kuju volcano and the city of Oita, where a NE–SW-trending structural boundary exists. Between such structural boundaries, Aso volcano exists with the local conductor. At depths of 8 and 12 km, the zone around the Futagawa and Hinagu faults (the Seis. 1 zone) becomes approximately resistive,

although the location of hypocenter of the Kumamoto earthquake was relatively conductive. The Aso and Kuju volcanoes are imaged as conductive zones. The Yufu, Tsurumi, and Garan volcanoes do not show a dominant conductor beneath them, while their southern part is imaged as a conductor. At a depth of 20 km, the northwestern parts of the Futagawa and Hinagu faults gradually become conductive again. This deep conductive zone is located beneath the region of Seis. 1, which extends to  $\sim 16$  km depth. The conductive zone beneath Aso volcano continues to depth, whereas the one beneath Kuju volcano moves to the west.

## Discussion

To investigate the relationship between the earthquakes and the resistivity structure in the study area, the hypocenters, which were relocated by manual readings of P-wave arrival times (Shimizu et al. 2016), are plotted on the resistivity sections at depths of 8 and 12 km (Fig. 6). Overall, the aftershocks (Seis. 1) were distributed mainly in the resistive zone (100–1000  $\Omega\text{m}$ ) at depths of 4–16 km beneath which the relatively conductive zones exist, especially to the northwest of Hinagu and Futagawa faults (Figs. 4, 6). The triggered earthquakes of Seis. 2 also occur in the resistive zone or the resistive-conductive transition zone. In 1975, an  $M_{\text{JMA}}$  6.1 earthquake occurred at approximately the same location, although its hypocentral depth is poorly determined (Yamashina and Murai 1975) (Fig. 6). In the region of Seis. 3, the triggered earthquakes also occurred in the relatively

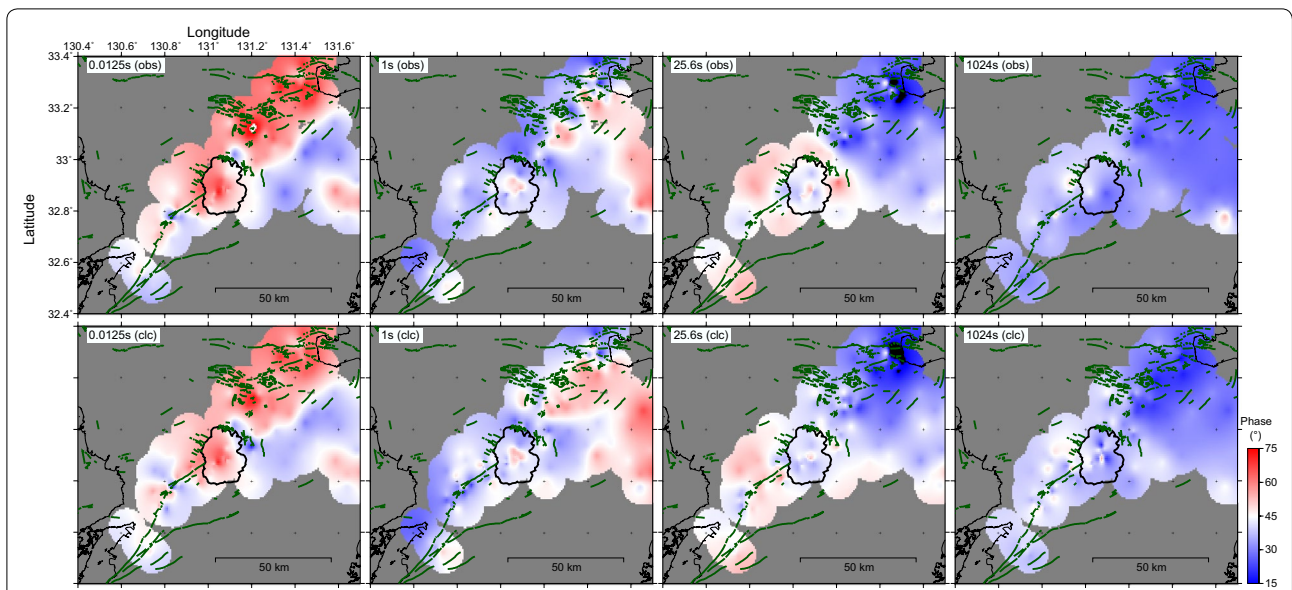


**Fig. 3** Phase map for comparison of observed data (obs) with calculated response (clc). Observational data with errors of  $>20^\circ$  are not shown. Other notations are the same as in Fig. 2

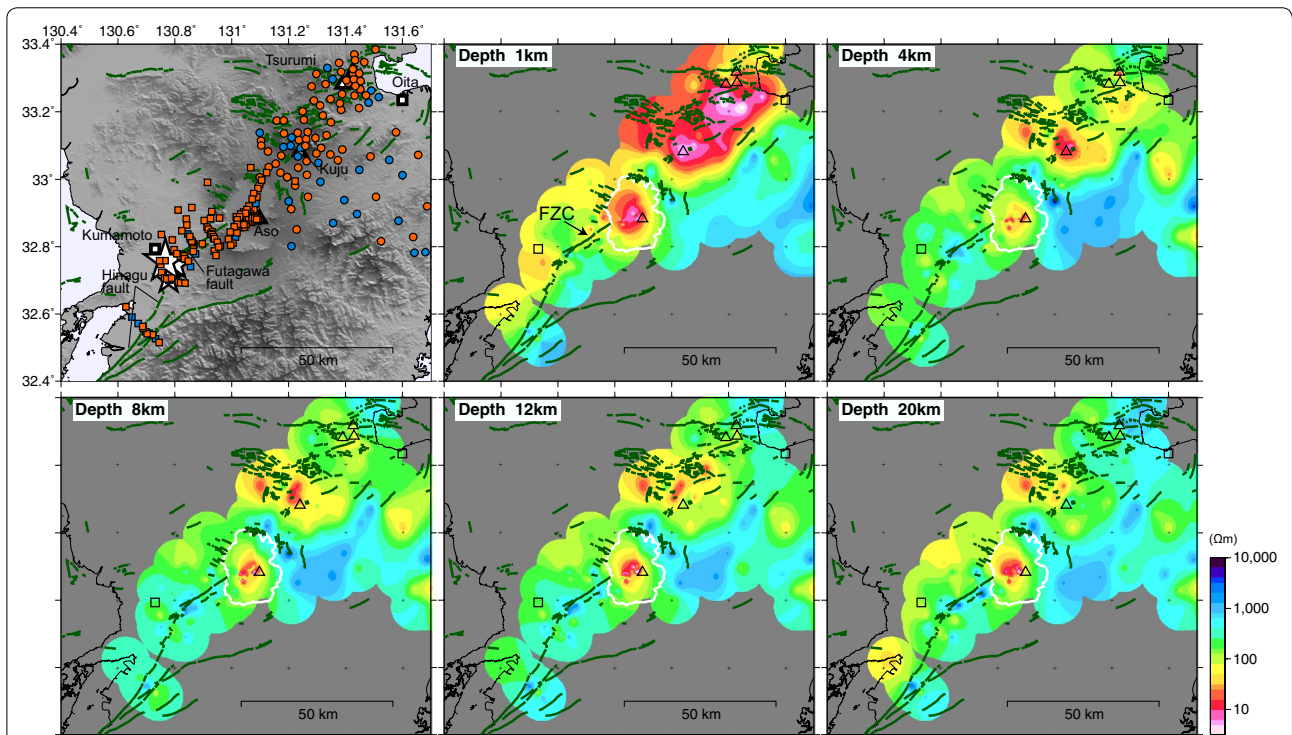
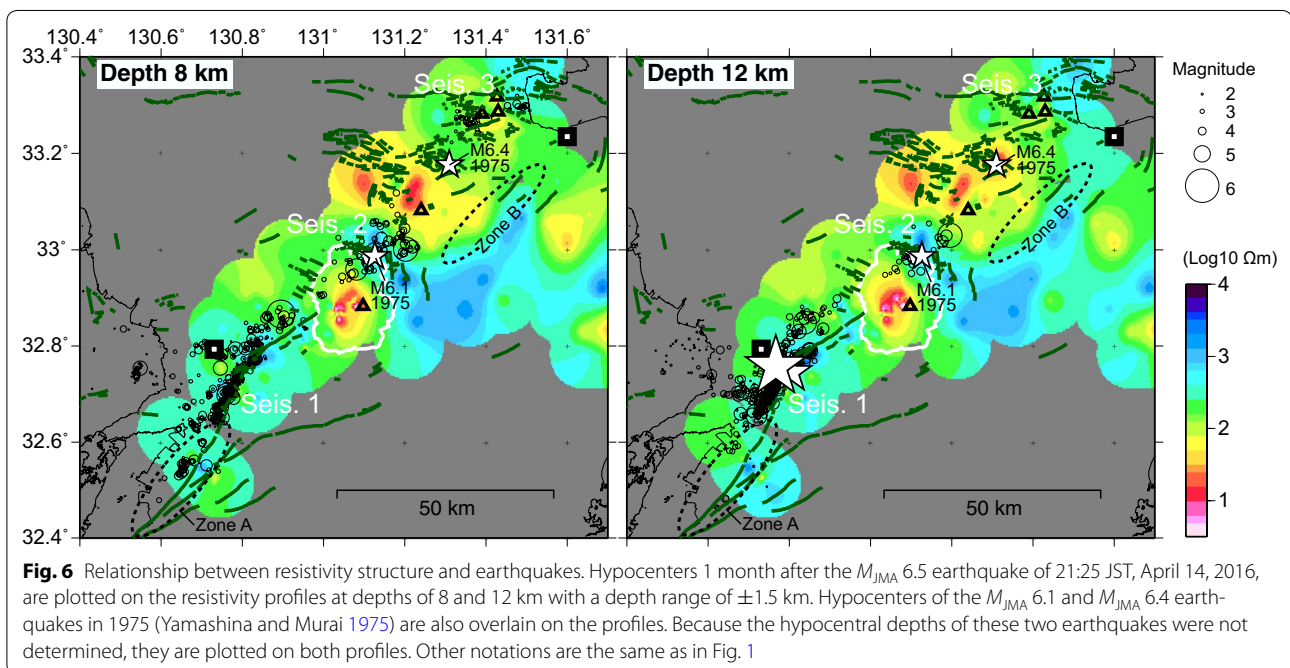
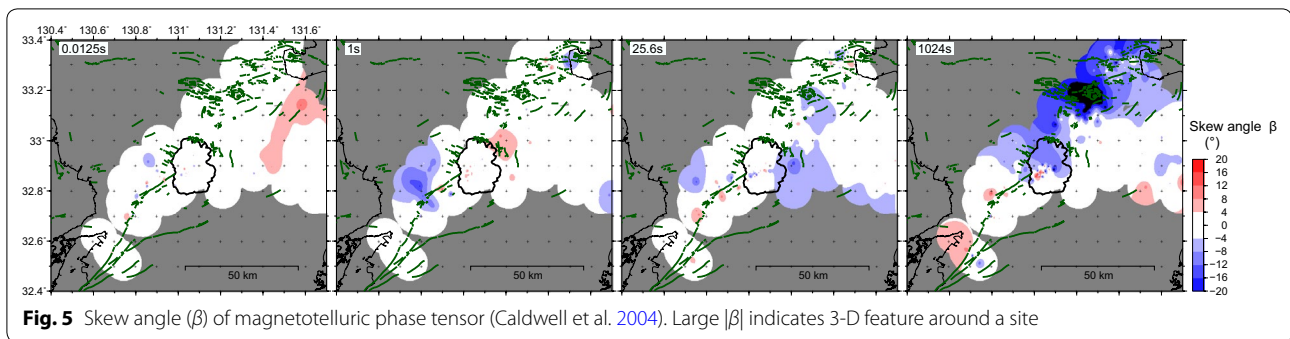


**Fig. 4** Resistivity structure estimated from the 1-D inversion. Other notations are the same as in Fig. 1. These maps were produced by interpolating the resistivities of 1-D structure at each site

resistive zones ( $>100 \Omega\text{m}$ ) west of Yufu volcano and east of Tsurumi volcano, or within the resistive-conductive transition zone, and in general avoid the surrounding

conductive ( $<100 \Omega\text{m}$ ) zones. Between Seis. 2 and Seis. 3, the hypocenter of the 1975  $M_{\text{JMA}}$  6.4 earthquake (Oita-Chubu earthquake) is located in a relatively resistive



zone, although its hypocentral depth is poorly determined (Yamashina and Murai 1975; Fukuoka District Meteorological Observatory 1976) (Fig. 6). In general, the earthquakes occur in electrically resistive zones adjacent to conductive zones or resistive-conductive transition zones, and seismicity is low in conductive zones.

Because the conductive zones are located in the middle crust in the vicinity of active volcanoes (Kuju, Aso, Tsurumi, Garan, and Yufu) or in the lower crust beneath the Futagawa and Hinagu faults, we interpret that the deep conductors represent high-temperature ductile or low-rigidity zones due to the presence of fluids such as magma or saline water. In contrast, we interpret the resistive zones as relatively cold brittle zones with a fluid

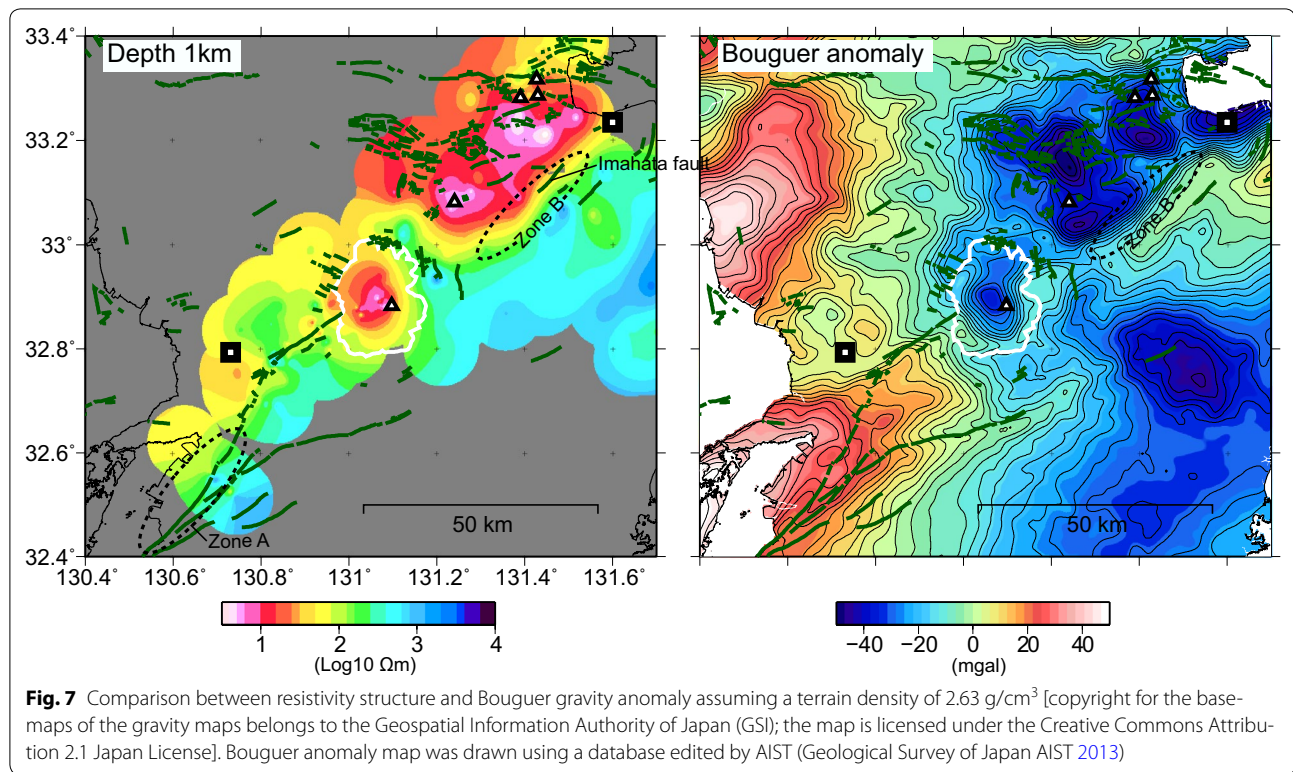
deficit. We hypothesize that the conductive zone preferentially deforms, such that the static stress over Kyushu (Matsumoto et al. 2015; Savage et al. 2016) accumulates preferentially in proximal brittle resistive zones and subsequently causes large earthquakes. The concept of local stress accumulation has been proposed based on the results of previous magnetotelluric studies (e.g., Ogawa et al. 2001; Ichihara et al. 2008, 2014; Wannamaker et al. 2009). The concept is similar to the hypothesis of Iio et al. (2002) who assumed that the lower crust had a deformable weak zone. In addition, our results suggest that fluids supplied from conductive zones to nearby resistive zones can promote earthquake occurrences (e.g., Mitsuhashi et al. 2001; Ogawa et al. 2001; Yoshimura et al.

2009) by increasing pore pressure and decreasing the effective normal stress. Although it is usually difficult to uniquely determine the triggering mechanism, the effect of fluids on earthquake generation is especially plausible in the region of Seis. 3, which is approximately 100 km away from the hypocenter of the  $M_{JMA}$  7.3 earthquake. Between the hypocenter of the main shock and Seis. 3 lies a remarkably conductive zone. In this case, the static stress change (e.g., Hardebeck et al. 1998) caused by the 2016 Kumamoto earthquake was not effectively transferred at distance, but instead, the dynamic effects of seismic shaking were considered to be reasonable earthquake triggers (Miyazawa 2016). Because Seis. 3 occurs beneath active volcanoes, gas-rich hydrothermal water and/or gas bubbles exist at depth beneath the region, and their upwelling could have been facilitated by ground motion leading to earthquakes (e.g., Hill and Prejean 2005; Aizawa et al. 2016) in the Seis. 3 region.

This study shows that the seismogenic zones correspond approximately to resistive zones lying adjacent to conductive zones, or to the conductive-resistive transition zone. These results are consistent with previous magnetotelluric studies conducted across the epicenters of large ( $>M$  6) inland earthquakes (Mitsuhashi et al. 2001; Ogawa et al. 2001; Tank et al. 2003, 2005; Kasaya and Oshiman 2004; Ichihara et al. 2008, 2014; Yoshimura et al. 2008; Kaya et al. 2009; Umeda et al. 2011, 2014; Chandrasekhar et al. 2012) with the exception that aftershocks occur in a thick sedimentary layer (Uyeshima et al. 2005). Note here that the dense magnetotelluric observations occasionally image localized subvertical conductors beneath the active faults (e.g., Unsworth et al. 1997; Wannamaker et al. 2002; Becken et al. 2008; Ikeda et al. 2013; Sass et al. 2014). These local conductors, which are termed fault zone conductors, were interpreted to be damaged zones characterized by a fluid filled fracture network and altered clay materials. Previous two-dimensional (2-D) inversions in the region of our dataset have imaged the vertical conductors with a width of 1–4 km beneath the Futagawa fault (Asaue et al. 2004). The 1-D inversion of this study also shows the local conductor along the Futagawa fault at a depth of 1 km (FZC in Fig. 4). In addition, Fig. 4 shows the local conductor with a resistivity of around 100  $\Omega$ m at the hypocenter of the main shock. To confirm the presence of such small-scale conductors and their relationship to the earthquakes, the collection of more magnetotelluric observations and 2-D and/or 3-D inversions is necessary.

Considering the relationship between resistivity structure and seismicity, we suggest that two zones (Zones A and B in Fig. 6) have similar structures to the zones of Seis. 1–Seis. 3. Zone A corresponds to the southern part of Hinagu fault, which is 10–50 km from the hypocenter of the main shock. Zone A includes a zone of high radon-222 concentration in soil gas, which suggests large gas ascent velocities caused by frequently induced strain along the Hinagu fault (Koike et al. 2014). Further, a conductive zone like Seis. 1 is suggested at depths of ~20 km beneath Zone A, and therefore, this region is considered to have a relatively high potential of earthquake generation. Indeed in 1619, a  $M$  6.2 earthquake occurred around Zone A (Usami 1967).

Zone B is located 70–100 km east-northeast of the mainshock hypocenter. Zone B has been classified as seismically inactive for the last 20 years (Matsumoto et al. 2015), and no earthquake was triggered by the 2016 Kumamoto earthquake (Figs. 1, 6). However, Zone B corresponds to the possible western extension of the MTL where a possibly active fault (the Imahata-Shiraie fault) is located (Research Group for Active Faults in Japan 1991). The resistivity structure shows the structural boundary in Zone B at depths of 1–12 km (Figs. 4, 6). To investigate the origin of the structural boundary, we compared the shallow resistivity structure with the gravity data. Figure 7 shows the resistivity structure at a depth of 1 km and the Bouguer anomaly, assuming a terrain density of 2.63 g/cm<sup>3</sup> (Geological Survey of Japan AIST 2013). The structural boundary of Zone B is well correlated to a zone with a steep gravity gradient, which is interpreted to be the southern rim of a graben structure (Kamata 1989; Kamata and Kodama 1994). Recent studies suggest that the graben is a pull-apart basin related to the MTL dextral movements partly with volcanic depressions (Itoh et al. 1998; Saiga et al. 2010; Itoh et al. 2014). The altered volcano-clastic rock and hydrothermal water filling the graben are considered to be the cause of the low resistivity at shallow levels. Although Itoh et al. (1998) and Itoh et al. (2014) suggest that Zone B is inactive at the present time, GPS data support active shear around this region (Nishimura and Hashimoto 2006; Wallace et al. 2009). The stress field estimated from earthquakes also supports aseismic slip at the shear zone (Matsumoto et al. 2015). Furthermore, Zone B corresponds to the edge of the conductor at depths of 8 and 12 km. Therefore, Zone B may have a high potential of occurrence of large earthquakes.



## Conclusions

1-D analysis of the resistivity structure constrained by the 247 broadband MT and telluric observation sites has clarified that the aftershocks and triggered earthquakes of the 2016 Kumamoto earthquake occurred on electrically resistive zones adjacent to conductive zones or resistive-conductive transition zones. Seismicity was found to be quite low in the electrically conductive zones that are interpreted to be fluidized. This relationship is consistent with previous MT studies of other seismogenic zones around the world. Therefore, we conclude that seismic hazard assessments may be improved by considering the resistivity structure.

We interpret the difference in resistivity to represent a difference in elastic properties. The release of stress that had accumulated within the resistive region in the vicinity of the resistive-conductive boundary, probably led to the series of earthquakes. Increases in pore pressure from fluids supplied from the conductive zone may have been an additional cause of the earthquakes. Future dense MT observations made around the Futagawa and Hinagu faults and 3-D inversion will contribute to improving the sharpness of resistivity structure images and will characterize seismicity more clearly from the viewpoint of its relationship with resistivity structure.

### Authors' contributions

KA, MU, ST, and NM designed the field survey for the new dataset and processed the time series data. HA, KK, ST, TH, and TY contributed to obtain

the previously published MT data and its interpretation. KA carried out the 1-D inversion and drafted the manuscript. All authors contributed to the MT data acquisition and discussion. All authors read and approved the final manuscript.

### Author details

- <sup>1</sup> Institute of Seismology and Volcanology, Faculty of Science, Kyushu University, 2-5643-29 Shin'yama, Shimabara, Nagasaki 855-0843, Japan.
- <sup>2</sup> Laboratory on Innovative Techniques for Infrastructures, Kyoto University, C3-b4515, Kyoto daigaku-katsura, Nishikyo-ku, Kyoto 615-8540, Japan.
- <sup>3</sup> Environmental Geosphere Engineering, Department of Urban Management, Graduate School of Engineering, Kyoto University, C1-2, Kyoto daigaku-katsura, Nishikyo-ku, Kyoto 615-8540, Japan.
- <sup>4</sup> Geological Survey of Japan, National Institute of Advanced Industrial Science and Technology, 1-1-1 Higashi, Tsukuba 305-8567, Japan.
- <sup>5</sup> Aso Volcanological Laboratory, Institute for Geothermal Sciences, Graduate School of Science, Kyoto University, Minamiaso, Aso, Kumamoto 869-1404, Japan.
- <sup>6</sup> Disaster Prevention Research Institute, Kyoto University, Gokasho, Uji, Kyoto 611-0011, Japan.
- <sup>7</sup> Miyazaki Observatory, Disaster Prevention Research Institute, Kyoto University, 3884 Kaeda, Miyazaki 889-2161, Japan.
- <sup>8</sup> Earthquake Research Institute, University of Tokyo, Yayoi 1-1-1, Bunkyo-ku, Tokyo 113-0032, Japan.
- <sup>9</sup> Volcanic Fluid Research Center, Tokyo Institute of Technology, Ookayama 2-12-2, Meguro-ku, Tokyo 152-8551, Japan.
- <sup>10</sup> Faculty of Engineering, Kumamoto University, 2-39-1 Kurokami, Kumamoto 860-8555, Japan.
- <sup>11</sup> Institute of Seismology and Volcanology, Hokkaido University, N10W8, Kita-ku, Sapporo 060-0810, Japan.
- <sup>12</sup> Hokkaido Research Organization, Environmental and Geological Research Department, Geological Survey Hokkaido, Kita 19-jo Nishi 12-chome, Kita-ku, Sapporo 060-0819, Japan.

### Acknowledgements

We are greatly indebted to the landowners for permitting access for field campaigns. The geomagnetic data used for the remote-reference processing were provided by the Kakioka Geomagnetic Observatory of the Japan Meteorological Agency and Esashi Observatory of the Geospatial Information Authority of Japan. Our gratitude goes to S. Constable for supplying his 1-D inversion code. We thank the students of Kyushu University for their assistance during the



field campaigns. Comments by two anonymous reviewers and the Associate Editor, M. Hashimoto, greatly improved the manuscript. This study was supported by the Ministry of Education, Culture, Sports, Science and Technology (MEXT) of Japan, under its "Earthquake and Volcano Hazards Observation and Research Program" and "Research on Active faults surveys" by the Headquarters for Earthquake Research Promotion. Observations for seismic data were partly supported by MEXT KAKENHI Grant Number 16H06298, MEXT under its Earthquake and Volcano Hazards Observation and Research Program, and Earthquake Research Institute, University of Tokyo, under Joint Usage Program.

#### Competing interests

The authors declare that they have no competing interests.

Received: 29 July 2016 Accepted: 17 December 2016

Published online: 03 January 2017

#### References

- Aizawa K, Koyama T, Uyeshima M, Hase H, Hashimoto T, Kanda W, Yoshimura R, Utsugi M, Ogawa Y, Yamazaki K (2013) Magnetotelluric and temperature monitoring after the 2011 sub-Plinian eruptions of Shinmoe-dake volcano. *Earth Planets Space* 65(6):539–550. doi:10.5047/eps.2013.05.008
- Aizawa K et al (2016) Gas pathways and remotely triggered earthquakes beneath Mount Fuji, Japan. *Geology* 44(2):127–130. doi:10.1130/g37313.1
- Shimizu H et al (2016) The 2016 Kumamoto Earthquake and related crustal activities. Paper presented at Japan Geoscience Union 2016 meeting, Makuhari Messe, Chiba, 20–25 May 2016
- Asano K, Iwata T (2016) Source rupture processes of the foreshock and mainshock in the 2016 Kumamoto earthquake sequence estimated from the kinematic waveform inversion of strong motion data. *Earth Planets Space* 68(1):147. doi:10.1186/s40623-016-0519-9
- Asaue H, Koike K, Takakura S, Yoshinaga T, Ohmi M (2004) Structural analysis of fracture zones in deep parts of an active fault using magnetotelluric survey. *Jpn Soc Eng Geol* 45(2):60–70 (in Japanese)
- Asaue H, Koike K, Yoshinaga T, Takakura S (2006) Magnetotelluric resistivity modeling for 3D characterization of geothermal reservoirs in the Western side of Mt. Aso, SW Japan. *J Appl Geophys* 58(4):296–312. doi:10.1016/j.jappgeo.2005.05.006
- Asaue H, Koike K, Yoshinaga T, Takakura S (2007) Characterizing deep resistivity structures of Futagawa-Hinagu faults belt and discussion on their relationship with micro-earthquakes distribution. *J Jpn Soc Eng Geol* 48(4):180–191 (in Japanese)
- Asaue H, Kubo T, Yoshinaga T, Koike K (2012) Application of magnetotelluric (MT) resistivity to imaging of regional three-dimensional geologic structures and groundwater systems. *Nat Resour Res* 21(3):383–393. doi:10.1007/s11053-012-9184-2
- Becken M, Ritter O, Park SK, Bedrosian PA, Weckmann U, Weber M (2008) A deep crustal fluid channel into the San Andreas fault system near Parkfield, California. *Geophys J Int* 173(2):718–732. doi:10.1111/j.1365-246X.2008.03754.x
- Caldwell TG, Bibby HM, Brown C (2004) The magnetotelluric phase tensor. *Geophys J Int*. doi:10.1111/j.1365-246X.2004.02281.x
- Chandrasekhar E, Mathew G, Harinarayana T (2012) A new hypothesis for the deep subsurface structures near the Bhuj 2001 earthquake (Mw 7.6) hypocentre zone and its tectonic implications. *Geophys J Int* 190(2):761–768. doi:10.1111/j.1365-246X.2012.05532.x
- Chave AD, Thomson DJ (2004) Bounded influence magnetotelluric response function estimation. *Geophys J Int* 157(3):988–1006. doi:10.1111/j.1365-246X.2004.02203.x
- Constable SC, Parker RL, Constable CG (1987) Occams inversion—a practical algorithm for generating smooth models from electromagnetic sounding data. *Geophysics* 52(3):289–300. doi:10.1190/1.1442303
- Fujinawa Y, Kawakami N, Inoue J, Aseh TH, Takasugi S (2002) Conductivity distribution and seismicity in the northeastern Japan Arc. *Earth Planets Space* 54(5):629–636. doi:10.1186/BF03353051
- Fukuoka District Meteorological Observatory (1976) Report on the Earthquake of Central Part of Oita, pref., April 21. *Q J Seismol* 40:81–103 (in Japanese)
- Gamble TD, Clarke J, Goubau WM (1979) Magnetotellurics with a remote magnetic reference. *Geophysics* 44(1):53–68
- Geological Survey of Japan AIST (2013) Gravity DataBase of Japan, DVD Edition. AIST, Tsukuba
- Goto TN, Wada Y, Oshiman N, Sumitomo N (2005) Resistivity structure of a seismic gap along the Atotsugawa Fault, Japan. *Phys Earth Planet Inter* 148(1):55–72. doi:10.1016/j.pepi.2004.08.007
- Guerer A, Bayrak M (2007) Relation between electrical resistivity and earthquake generation in the crust of West Anatolia, Turkey. *Tectonophysics* 445(1–2):49–65. doi:10.1016/j.tecto.2007.06.009
- Handa S (2005) Electrical conductivity structures estimated by thin sheet inversion, with special attention to the Beppu-Shimabara graben in central Kyushu, Japan. *Earth Planets Space* 57(7):605–612. doi:10.1186/BF03351839
- Handa S, Tanaka Y, Suzuki A (1992) The electrical high conductivity layer beneath the northern Okinawa trough, inferred from geomagnetic depth sounding in northern and central Kyushu, Japan. *J Geomagn Geoelectr* 44(7):505–520. doi:10.1186/BF03351839
- Hardebeck JL, Nazareth JJ, Hauksson E (1998) The static stress change triggering model: constraints from two southern California after-shock sequences. *J Geophys Res Solid Earth* 103(B10):24427–24437. doi:10.1029/98jb00573
- Hata M, Takakura S, Matsushima N, Hashimoto T, Utsugi M (2016) Crustal magma pathway beneath Aso caldera inferred from three-dimensional electrical resistivity structure. *Geophys Res Lett* 43:10720–10727. doi:10.1002/2016GL070315
- Hill DP, Prejean S (2005) Magmatic unrest beneath Mammoth Mountain, California. *J Volcanol Geotherm Res* 146(4):257–283. doi:10.1016/j.jvolgeores.2005.03.002
- Ichihara H, Honda R, Mogi T, Hase H, Kamiyama H, Yamaya Y, Ogawa Y (2008) Resistivity structure around the focal area of the 2004 Rumoi-Nanbu earthquake (M 6.1), northern Hokkaido, Japan. *Earth Planets Space* 60(8):883–888. doi:10.1186/BF03352841
- Ichihara H et al (2011) A fault-zone conductor beneath a compressional inversion zone, northeastern Honshu, Japan. *Geophys Res Lett*. doi:10.1029/2011gl047382
- Ichihara H, Sakanaka S, Mishina M, Uyeshima M, Nishitani T, Ogawa Y, Yamaya Y, Mogi T, Amata K, Miura T (2014) A 3-D electrical resistivity model beneath the focal zone of the 2008 Iwate–Miyagi Nairiku earthquake (M 7.2). *Earth Planets Space* 66:50. doi:10.1186/1880-5981-66-50
- Ichihara H, Mogi T, Tanimoto K, Yamaya Y, Hashimoto T, Uyeshima M, Ogawa Y (2016) Crustal structure and fluid distribution beneath the southern part of the Hidaka collision zone revealed by 3-D electrical resistivity modeling. *Geochem Geophys Geosyst* 17(4):1480–1491. doi:10.1002/2015gc006222
- Iio Y, Sagiya T, Kobayashi Y, Shiozaki I (2002) Water-weakened lower crust and its role in the concentrated deformation in the Japanese Islands. *Earth Planet Sci Lett* 203(1):245–253. doi:10.1016/s0012-821x(02)00879-8
- Ikeda M, Kato S, Nishizaka N, Ohno Y, Matsuo K, Kishimoto M (2013) Magnetotelluric imaging of the Median Tectonic Line in western Shikoku, southwest Japan: implications of the fault-related low-resistivity zone. *Tectonophysics* 601:78–86. doi:10.1016/j.tecto.2013.04.026
- Itoh Y, Takemura K, Kamata H (1998) History of basin formation and tectonic evolution at the termination of a large transcurrent fault system: deformation mode of central Kyushu, Japan. *Tectonophysics* 284(1–2):135–150. doi:10.1016/s0040-1951(97)00167-4
- Itoh Y, Kusumoto S, Takemura K (2014) Evolutionary process of Beppu Bay in central Kyushu, Japan: a quantitative study of the basin-forming process controlled by plate convergence modes. *Earth Planets Space* 66:74. doi:10.1186/1880-5981-66-74
- Kamata H (1989) Volcanic and structural history of the Hoho volcanic zone, central Kyushu, Japan. *Bull Volcanol* 51(5):315–332. doi:10.1007/bf01056894
- Kamata H, Kodama K (1994) Tectonics of an arc arc junction—an example from Kyushu Island at the junction of the southwest Japan arc and the Ryukyu arc. *Tectonophysics* 233(1–2):69–81. doi:10.1016/0040-1951(94)90220-8
- Kanaori Y, Kawakami S, Yairi K (1994) Seismotectonics of the Median Tectonic Line in southwest Japan—implications for coupling among major fault systems. *Pure Appl Geophys* 142(3–4):589–607. doi:10.1007/bf00876056

- Kasaya T, Oshiman N (2004) Lateral inhomogeneity deduced from 3-D magnetotelluric modeling around the hypocentral area of the 1984 Western Nagano Prefecture earthquake, central Japan. *Earth Planets Space* 56(5):547–552. doi:[10.1186/BF03352514](https://doi.org/10.1186/BF03352514)
- Kaya T, Tank SB, Tuncer MK, Rokoityansky II, Tolak E, Savchenko T (2009) Asperity along the North Anatolian Fault imaged by magnetotellurics at Duzce, Turkey. *Earth Planets Space* 61(7):871–884. doi:[10.1186/BF03353198](https://doi.org/10.1186/BF03353198)
- Kaya T, Kasaya T, Tank SB, Ogawa Y, Tuncer MK, Oshiman N, Honkura Y, Matsushima M (2013) Electrical characterization of the North Anatolian Fault Zone underneath the Marmara Sea, Turkey by ocean bottom magnetotellurics. *Geophys J Int* 193(2):664–677. doi:[10.1093/gji/ggt025](https://doi.org/10.1093/gji/ggt025)
- Kelbert A, Meqbel N, Egbert GD, Tandon K (2014) ModEM: a modular system for inversion of electromagnetic geophysical data. *Comput Geosci* 66:40–53. doi:[10.1016/j.cageo.2014.01.010](https://doi.org/10.1016/j.cageo.2014.01.010)
- Kobayashi H, Koketsu K, Miyake H (2016) Rupture processes of the 2016 Kumamoto earthquakes derived from joint inversion of strong-motion, teleseismic, and geodetic data. Paper presented at Japan Geoscience Union 2016 meeting, Makuu-hari Messe, Chiba, 20–25 May 2016
- Koike K, Yoshinaga T, Ueyama T, Asaue H (2014) Increased radon-222 in soil gas because of cumulative seismicity at active faults. *Earth Planets Space* 66:57. doi:[10.1186/1880-5981-66-57](https://doi.org/10.1186/1880-5981-66-57)
- Matsumoto Y (1979) Some problems on volcanic activities and depression structures in Kyushu, Japan. *Mem Geol Soc Jpn* 16:127–139 (**in Japanese**)
- Matsumoto S, Nakao S, Ohkura T, Miyazaki M, Shimizu H, Abe Y, Inoue H, Nakamoto M, Yoshikawa S, Yamashita Y (2015) Spatial heterogeneities in tectonic stress in Kyushu, Japan and their relation to a major shear zone. *Earth Planets Space* 67:172. doi:[10.1186/s40623-015-0342-8](https://doi.org/10.1186/s40623-015-0342-8)
- Mitsuhashi Y, Ogawa Y, Mishina M, Kono T, Yokokura T, Uchida T (2001) Electromagnetic heterogeneity of the seismogenic region of 1962 M6.5 northern Miyagi earthquake, northeastern Japan. *Geophys Res Lett* 28(23):4371–4374
- Miyazaki S, Heki K (2001) Crustal velocity field of southwest Japan: subduction and arc-arc collision. *J Geophys Res Solid Earth* 106(B3):4305–4326. doi:[10.1029/2000jb900312](https://doi.org/10.1029/2000jb900312)
- Miyazawa M (2016) An investigation into the remote triggering of the Oita earthquake by the 2016 Mw 7.0 Kumamoto earthquake using full wavefield simulation. *Earth Planets Space* 68:205. doi:[10.1186/s40623-016-0585-z](https://doi.org/10.1186/s40623-016-0585-z)
- Nishimura S, Hashimoto M (2006) A model with rigid rotations and slip deficits for the GPS-derived velocity field in Southwest Japan. *Tectonophysics* 421(3–4):187–207. doi:[10.1016/j.tecto.2006.04.017](https://doi.org/10.1016/j.tecto.2006.04.017)
- Ogawa Y et al (2001) Magnetotelluric imaging of fluids in intraplate earthquake zones, NE Japan back arc. *Geophys Res Lett* 28(19):3741–3744
- Ogawa Y, Ichiki M, Kanda W, Mishina M, Asamori K (2014) Three-dimensional magnetotelluric imaging of crustal fluids and seismicity around Naruko volcano, NE Japan. *Earth Planets Space* 66:158. doi:[10.1186/s40623-014-0158-y](https://doi.org/10.1186/s40623-014-0158-y)
- Research Group for Active Faults in Japan (1991) Active faults in Japan. Sheet maps and inventories. University of Tokyo Press, Tokyo
- Rung-Arunwan T, Siripunvaraporn W, Utada H (2016) On the Berdichevsky average. *Phys Earth Planet Inter* 253:1–4. doi:[10.1016/j.pepi.2016.01.006](https://doi.org/10.1016/j.pepi.2016.01.006)
- Saiga A, Matsumoto S, Uehira K, Matsushima T, Shimizu H (2010) Velocity structure in the crust beneath the Kyushu area. *Earth Planets Space* 62(5):449–462. doi:[10.5047/eps.2010.02.003](https://doi.org/10.5047/eps.2010.02.003)
- Sass P, Ritter O, Ratschbacher L, Tympl J, Matiukov VE, Rybin AK, Batalev VY (2014) Resistivity structure underneath the Pamir and Southern Tian Shan. *Geophys J Int* 198(1):564–579. doi:[10.1093/gji/ggu146](https://doi.org/10.1093/gji/ggu146)
- Savage MK, Aoki Y, Unglert K, Ohkura T, Umakoshi K, Shimizu H, Iguchi M, Tameguri T, Ohminato T, Mori J (2016) Stress, strain rate and anisotropy in Kyushu, Japan. *Earth Planet Sci Lett* 439:129–142. doi:[10.1016/j.epsl.2016.01.005](https://doi.org/10.1016/j.epsl.2016.01.005)
- Seno T (1999) Syntheses of the regional stress fields of the Japanese islands. *Isl. Arc* 8(1):66–79. doi:[10.1046/j.1440-1738.1999.00225.x](https://doi.org/10.1046/j.1440-1738.1999.00225.x)
- Seno T, Stein S, Gripp AE (1993) A Model for the motion of the Philippine sea plate consistent with NUVEL-1 and geological data. *J Geophys Res Solid Earth* 98(B10):17941–17948. doi:[10.1029/93jb00782](https://doi.org/10.1029/93jb00782)
- Shimoizumi M, Mogi T, Nakada M, Yukutake T, Handa S, Tanaka Y, Utada H (1997) Electrical conductivity anomalies beneath the western sea of Kyushu, Japan. *Geophys Res Lett* 24(13):1551–1554. doi:[10.1029/97gl01542](https://doi.org/10.1029/97gl01542)
- Siripunvaraporn W, Egbert G (2009) WSINV3DMT: vertical magnetic field transfer function inversion and parallel implementation. *Phys Earth Planet Inter* 173(3–4):317–329. doi:[10.1016/j.pepi.2009.01.013](https://doi.org/10.1016/j.pepi.2009.01.013)
- Szarka L, Menvielle M (1997) Analysis of rotational invariants of the magnetotelluric impedance tensor. *Geophys J Int* 129(1):133–142. doi:[10.1111/j.1365-246X.1997.tb00942.x](https://doi.org/10.1111/j.1365-246X.1997.tb00942.x)
- Tabei T et al (2002) Subsurface structure and faulting of the Median Tectonic Line, southwest Japan inferred from GPS velocity field. *Earth Planets Space* 54(11):1065–1070. doi:[10.1186/BF03353303](https://doi.org/10.1186/BF03353303)
- Takakura S, Hashimoto T, Koike K, Ogawa Y (2000) Resistivity sections of the Aso caldera, central Kyushu, Japan (in Japanese), Papers on conductivity anomaly research group 23–30
- Tank SB, Honkura Y, Ogawa Y, Oshiman N, Tuncer MK, Matsushima M, Celik C, Tolak E, Isikara AM (2003) Resistivity structure in the western part of the fault rupture zone associated with the 1999 Izmit earthquake and its seismogenic implication. *Earth Planets Space* 55(7):437–442. doi:[10.1186/BF03351777](https://doi.org/10.1186/BF03351777)
- Tank SB, Honkura Y, Ogawa Y, Matsushima M, Oshiman N, Tuncer MK, Celik C, Tolak E, Isikara AM (2005) Magnetotelluric imaging of the fault rupture area of the 1999 Izmit (Turkey) earthquake. *Phys Earth Planet Inter* 150(1–3):213–225. doi:[10.1016/j.pepi.2004.08.033](https://doi.org/10.1016/j.pepi.2004.08.033)
- Toda S, Nishizaka N, Onishi K, Suzuki S (2015) Progressive failure during the 1996 Keicho earthquakes on the Median Tectonic Line active fault zone, southwest Japan. AGU fall meeting, San Francisco
- Umeda K, Asamori K, Negi T, Kusano T (2011) A large intraplate earthquake triggered by latent magmatism. *J Geophys Res Solid Earth*. doi:[10.1029/2010jb007963](https://doi.org/10.1029/2010jb007963)
- Umeda K, Asamori K, Makuuchi A, Kobori K (2014) Earthquake doublet in an active shear zone, southwest Japan: constraints from geophysical and geochemical findings. *Tectonophysics* 634:116–126. doi:[10.1016/j.tecto.2014.07.025](https://doi.org/10.1016/j.tecto.2014.07.025)
- Unsworth MJ, Malin PE, Egbert GD, Booker JR (1997) Internal structure of the San Andreas fault at Parkfield, California. *Geology* 25(4):359–362
- Usami T (1967) Descriptive table of major earthquakes in and near Japan which were accompanied by damages. *Bull Earthq Res Inst Univ Tokyo* 44:1571–1622
- Uyeshima M et al (2005) Resistivity imaging across the source region of the 2004 Mid-Niigata Prefecture earthquake (M6.8), central Japan. *Earth Planets Space* 57(5):441–446. doi:[10.1186/BF03351831](https://doi.org/10.1186/BF03351831)
- Wallace LM, Ellis S, Miyao K, Miura S, Beavan J, Goto J (2009) Enigmatic, highly active left-lateral shear zone in southwest Japan explained by aseismic ridge collision. *Geology* 37(2):143–146. doi:[10.1130/g25221a.1](https://doi.org/10.1130/g25221a.1)
- Wannamaker PE, Jiracek GR, Stodt JA, Caldwell TG, Gonzalez VM, McKnight JD, Porter AD (2002) Fluid generation and pathways beneath an active compressional orogen, the New Zealand Southern Alps, inferred from magnetotelluric data. *J Geophys Res Solid Earth*. doi:[10.1029/2001JB00186](https://doi.org/10.1029/2001JB00186)
- Wannamaker PE, Caldwell TG, Jiracek GR, Maris V, Hill GJ, Ogawa Y, Bibby HM, Bennie SL, Heise W (2009) Fluid and deformation regime of an advancing subduction system at Marlborough, New Zealand. *Nature* 460(7256):U733–U790. doi:[10.1038/nature08204](https://doi.org/10.1038/nature08204)
- Yamashina K, Murai I (1975) On the focal mechanism of the earthquakes in the central part of Oita prefecture and in the northern part of Aso of 1975, especially, the relation to the active fault system. *Bull Earthq Res Int* 50:295–302
- Yoshimura R et al (2008) Magnetotelluric observations around the focal region of the 2007 Noto Hanto Earthquake (M<sub>s</sub> 6.9), Central Japan. *Earth Planets Space* 60(2):117–122. doi:[10.1186/BF03352771](https://doi.org/10.1186/BF03352771)
- Yoshimura R et al (2009) Magnetotelluric transect across the Niigata-Kobe Tectonic Zone, central Japan: a clear correlation between strain accumulation and resistivity structure. *Geophys Res Lett*. doi:[10.1029/2009gl040016](https://doi.org/10.1029/2009gl040016)